Autonomous Nested Search for Hydrothermal Venting

Andrew Branch[1], Guangyu Xu[2], Michael V. Jakuba[2], Christopher R. German[2], Steve Chien[1], James C. Kinsey[2], Andrew D. Bowen[2], Kevin P. Hand[1], Jeffrey S. Seewald[2]

[1]Jet Propulsion Laboratory, California Institute of Technology

[2]Woods Hole Oceanographic Institution

Correspondence Author: andrew.branch@jpl.nasa.gov

Abstract

Ocean Worlds represent one of the best chances for the discovery of extra-terrestrial life within our own solar system. Liquid oceans are thought to exist on these celestial bodies, often encased in a thick icy shell. In order to investigate these oceans, a new mission concept utilizing a submersible craft must be developed. This vehicle would be required to traverse the icy shell and travel hundreds or even thousands of kilometers to survey the ocean below. In doing this, the vehicle might be out of contact for weeks or months at a time, requiring it to autonomously detect, locate, and study features of interest. Hydrothermal venting is one potential target, due to the unique ecosystems it supports on Earth. We have developed an autonomous, nested search strategy to locate sources of hydrothermal venting based on currently used methods. To test this search technique a simulation environment was developed using a hydrothermal plume dispersion simulation and a vehicle model. We show the effectiveness of the search method in this environment.

Introduction

At least eight bodies in our solar system are thought to harbor liquid oceans. In some cases, such as Europa and Enceladus, this ocean is perhaps habitable and encased in an icy shell kilometers thick [National Aeronautics and Space Administration 2018]. To explore these worlds new mission concepts must be developed using penetrating, submersible vehicles. A notional mission concept for such a submersible, outlined in Figure 1, contains four main components, an orbiting communications relay, a surface antenna, an under-ice base station, and a submersible vehicle. In order to facilitate ice shell transit, the vehicle needs to be small (particularly in cross sectional area). The long mission duration — potentially over a year to melt through the icy shell and a one year exploration mission — requires a low power vehicle, limiting the types of instruments on board. While the vehicle would ideally travel hundreds to thousands of kilometers distant from the base station, the submersible would need to return close to the base station to transfer data – with data subsequently relayed from the base station, through the surface antenna to the orbiter for eventual return to Earth. The radiation environment near the target body could preclude the use of an orbiting communication relay, instead relying on a relay in an eccentric Jovian orbit, in the case of Europa, increasing the time between communication windows from daily to monthly. When the submersible is away from the base station it would be unable to communicate with Earth. Therefore, while making journeys further and further away from the base station, the submersible might be operating days or weeks without contact. During this time the submersible would be required to autonomously detect, locate, and study a specific feature of interest.

Hydrothermal venting is one potential target for a submersible mission. Evidence for hydrothermal activity has been found on one Ocean World, Enceladus [Hsu et al. 2015; Waite et al. 2017]. On Earth, these geological phenomena harbor unique ecosystems and are potentially critical to the origin of life. Similar vents on Ocean Worlds could be the best chance at extra-terrestrial life in our Solar System. We have developed a fully autonomous nested search strategy for the localization of hydrothermal vents based on a manual three-phase nested search commonly used in the field [German et al. 2008]. In order to test this approach we have developed a simulation environment using FVCOM [Chen, Liu, and Beardsley 2003] — an existing ocean circulation model — and a vehicle model. Due to the resolution of the simulation environment, we focus on search in the non-buoyant plume. This corresponds to the ship based CTD casts and the phase 1 survey of the method presented in [German et al. 2008].

The rest of the paper is organized as follows. First we discuss the structure of hydrothermal venting. Then we discuss the simulation environment used to test our approach. We outline the approach itself and the experimental setup. Finally we discuss the results and future work.

Related Work

Adaptive sampling and control of autonomous underwater vehicles has been extensively studied, including foundational work with the Autonomous Ocean Sampling Network [Curtin et al. 1993; Curtin and Bellingham 2009; Ramp et al. 2009; Haley et al. 2009; Leonard et al. 2007].

Hydrothermal vent localization on Earth is often done with a non-autonomous three-phase nested search [German et al. 2008]. [Yoerger et al. 2007a] demonstrates this method in a number of cruises. [Yoerger et al. 2007b] presents a method to autonomously revisit areas of interest after the primary mission is completed, however this requires humans to develop the primary mission. This method was used in the

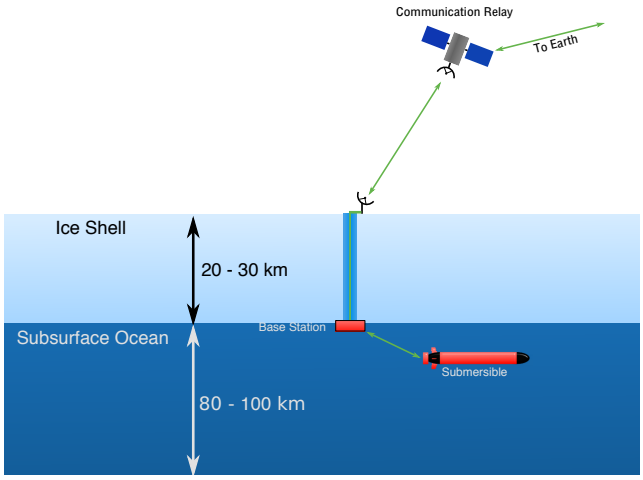

Figure 1: Notional Europa submersible mission showing the communication pathway from the submersible vehicle to Earth. Approximate ice thickness and ocean depth are labeled.

field multiple times. [Farrell, Pang, and Li 2005] field tests a strategy inspired by moths in order to trace chemical plumes.

Many approaches have been tested in idealized simulation environments or with deployment data, which does not allow for testing of fully autonomous planning algorithms. [Pang 2010] and [Tian et al. 2014] use moth based strategies in order to localize hydrothermal venting. [Jakuba and Yoerger 2008] uses occupancy grid mapping in order to localize vents. [Saigol et al. 2010] uses a belief-maximization algorithm to find a target of interest in simulation. [Ferri, Jakuba, and Yoerger 2010] uses a trigger based approach in order to gather higher resolution data in areas of strong sensor readings.

Hydrothermal venting is not the only target of interest. While not all ocean processes on Earth are expected to recur on other ocean worlds distant from the sun, we have a wealth of experience studying thermoclines, ocean fronts, and other structures in Earth's oceans. A number of different near real-time feature tracking methods exist for thermoclines [Cruz and Matos 2010; Zhang et al. 2010; Sun et al. 2016]. [Zhang et al. 2013; 2016] tracks upwelling fronts using a zig-zag pattern. [Cruz and Matos 2014] tracks any gradient boundary using a single vehicle following a dynamic zig-zag pattern and a lateral gradient detection algorithm to estimate the gradient boundary using an arc. A similar method can also be applied to tracking the center of a phytoplankton bloom patch [Godin et al. 2011]. [Branch et al. 2018] uses near real-time data to autonomously retask a set of vehicles to repeatedly sample an ocean front. Machine learning, in the form of policy learning, has been applied to the problem of tracking the edge of a harmful algal bloom [Magazzeni et al. 2014]. Other work focuses on tracking algal blooms by flying formations relative to the bloom as tracked by a drifter [Das et al. 2012]. [Petillo, Schmidt, and Balasuriya 2012] uses a simulated network of AUVs in order to estimate the boundary of a simulated plume. [Flexas et al. 2018] uses an ocean model and autonomous planning to optimize sampling of submesoscale structures.

Onboard autonomy has also been used to coordinate multiple vehicles and correct for ocean currents. The Adaptive Sampling and Prediction project [Leonard et al. 2010] used adaptive control to coordinate 6 gliders flying in loops at fixed spacing. [Troesch et al. 2016] uses an ocean model in order to improve the station keeping ability of vertically profiling floats. [Eriksen et al. 2001] describes the capabilities of a Seaglider to compensate for drift from currents using depth averaged currents over multiple dives.

Hydrothermal Venting

Hydrothermal venting produces a plume which can be traced back to the source. The structure of the plume is shown in Figure 2. Hydrothermal fluid exiting the vent is less dense than the surrounding water, resulting in the formation of a buoyant plume. Due to entrainment, the plume is continuously diluted by the ambient water column and expands from ~10 cm at the vent source to ~100 m at equilibrium. Upon reaching equilibrium, the plume expands horizontally — ten to hundreds of kilometers — to form the non-buoyant plume [German and Seyfried 2014]. The non-buoyant plume height is a function of the properties of the hydrothermal vent fluid as well as the surrounding water column [Turner 1979]. In the Pacific the non-buoyant plume is normally observed at 100-150 m above the seafloor, while in the Atlantic it is normally closer to 200-400 m [Speer and Rona 1989].

Hydrothermal plumes are the main source of information when localizing venting. However, tidal flows lead to local maxima [Veirs 2003], turbulent flow disrupting smooth gradients, differing vent types and strengths, and an unknown number of sources increase the difficulty of determining the plume source. [German et al. 2008] uses three primary sensors in the detection of hydrothermal plumes: temperature, optical backscatter [Baker, German, and Elderfield 1995; Baker and German 2004], and a chemical sensor such as oxidation-reduction potential [Nakamura et al. 2000]. These sensors may be good candidates for inclusion on a submersible mission to an Ocean World due to their compact form factor (100s of grams) and low power consumption (10s of milliwatts).

Simulation

A simulation environment was developed, using a hydrothermal plume dispersion simulation and a vehicle model. A numerical simulation of hydrothermal plume dispersion is performed using FVCOM, an ocean-circulation model, at Axial Seamount on the Juan de Fuca Ridge. The abundant lava supply to Axial supports vigorous hydrothermal systems and frequent volcanic activity, which have drawn extensive on-going scientific research that makes Axial one of the best-studied seamounts on this planet. A snapshot of this simulation is shown in Figures 3 and 4.

FVCOM is a finite-volume, time and density-dependent, three-dimensional, ocean circulation model [Chen, Liu, and

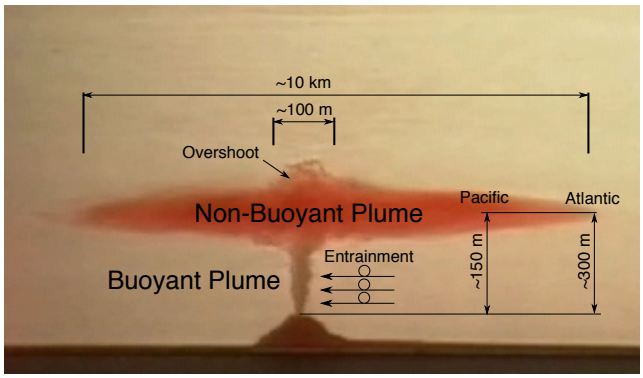

Figure 2: Demonstration of a hydrothermal plume performed in an aquarium tank. The buoyant and non-buoyant components of the hydrothermal vent plume are labeled with approximate scales. Image courtesy of C. German, WHOI

Beardsley 2003]. The unstructured grid employed in FVCOM supports grid size variation, therefore, proves efficient for the simulation of motion over a broad range of length scales. In addition, FVCOM supports the use of large-scale ocean circulation and tidal model outputs as open boundary forcing to drive flow across a broad range of frequencies inside the model domain [Zheng and Weisberg 2012].

Our model domain covers 300 by 300 km, centered on the Axial Seamount caldera and is open to flow across all four sides of that region. Horizontal resolution varies from 200 m within a 10 by 10km region enclosing Axial's caldera to 10km at the domain's boundary. The vertical dimension utilizes a uniform sigma-coordinate system with 127 layers, covering the full water column. This results in a ~12 m layer thickness above Axial's summit. The duration of the simulation is 58 days with model outputs sampled hourly. The 3-hourly sampled, 1/12.5° horizontal resolution, global reanalysis outputs of the HYbrid Coordinate Ocean Model (HYCOM) are used to construct the initial stratification profiles and open boundary forcing. Because HYCOM does not include ocean tides, we superimpose the tidal elevation and velocity predicted by the OSU Tidal Inversion onto the HYCOM outputs when constructing the open boundary forcing. We also add surface wind forcing and heat flux from 1-hourly sampled National Centers for Environmental Prediction (NCEP) Climate Forecast System Reanalysis (CFSR) outputs. We apply a linear ramp to bring open boundary and surface forcing from zero to full value over an initial four simulation days. Lastly, we add a seafloor heat source of 1 GW at the center (0,0) of the model domain inside Axial's caldera, which is turned on after the initial four simulation days. The model output consists of current, temperature, salinity, and a passive tracer, dye, which is released at the vent source. This tracer has a value range of $[0, 100]$. After 30 days the tracer content in a 20 by 20 km region surrounding the vent source reaches a quasi-steady state. In a 50 by 50 km region surrounding the vent source no quasi-steady state is reached before the end of the simulation.

The simulated vehicle uses a kinematic model and has three degrees-of-freedom: surge, heave, and yaw. A proportional controller allows the vehicle to navigate to a specified location. The nominal vehicle speed is set to 1 m/s. Simulated sensors are used to measure temperature, salinity, the passive tracer, vehicle depth, and distance to seafloor at a fixed interval. The position of the vehicle is assumed to be known at all times. Currently a chemical sensor, such as oxidation-reduction potential, and vehicle resources, such as energy and data capacity, are not modeled.

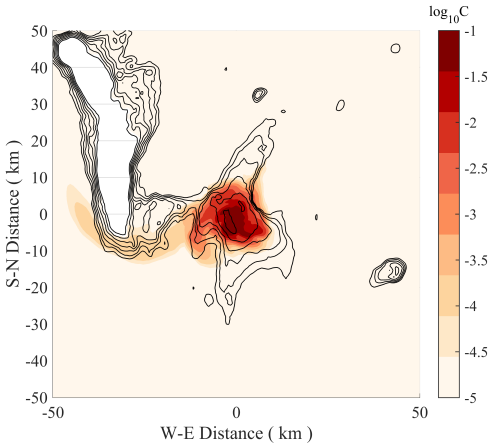

Figure 3: Snapshot taken at 1400 m depth on Mar 1, 2011 00:00 UTC of the simulated concentration (normalized by the source value) of a neutrally buoyant tracer originating from a hydrothermal vent source of 1 GW heat flux located inside the caldera of Axial Seamount at coordinate center. The global-simulation results of HYCOM and OSU Tidal Inversion for the period of Feb-Mar 2011 were used to drive flow inside the domain from its four boundaries.

Spatial Nested Search Strategy

Given a vehicle's starting location, the goal is to produce a control strategy that results in locating the vent source. The vent source is considered found when the region around the vent has been surveyed at a specified resolution. A resolution of 200 m was selected to match the resolution of the hydrothermal plume dispersion model at the vent source.

The strategy developed here addresses a number of issues. It mimics the field-proven methods of [German et al. 2008].

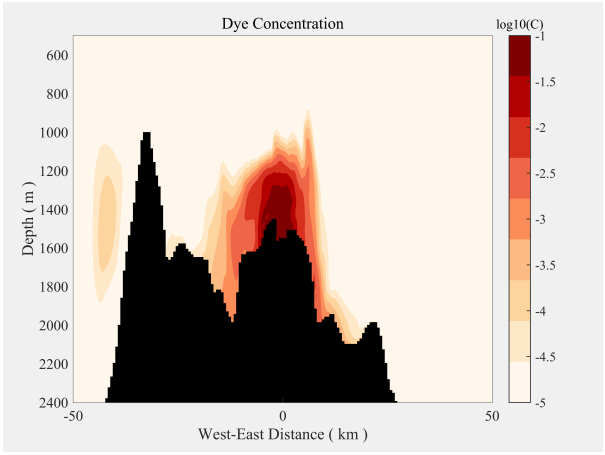

Figure 4: Snapshot taken along a W-E transect across the center of the model domain on Mar 1, 2011 00:00 UTC of the simulated concentration (normalized by the source value) of a neutrally buoyant tracer originating from a hydrothermal vent source of 1000 MW heat flux located inside the caldera of Axial Seamount at coordinate center. The global-simulation results of HYCOM and OSU Tidal Inversion for the period of Feb-Mar 2011 were used to drive flow inside the domain from its four boundaries.

Due to the limited resolution of the simulation environment, we focus specifically on search in the non-buoyant plume. (The buoyant plume is approximately 100 m, placing it below our 200 m resolution at the vent source.) This corresponds to the ship based CTD casts and — to some extent — phase 1 of the [German et al. 2008] method. Our strategy also allows for the localization of plume sources with differing strengths and maintains a robustness to local maxima in vent fluid concentrations and to small scale turbulence.

Before we can search for hydrothermal venting, we must have some method for detecting plumes. Ideally this would involve modeled sensors for temperature, optical backscatter, and oxidation reduction potential. However, currently we only use the passive tracer in the model as a direct measure of the hydrothermal plume. This is an area of future improvement.

The search algorithm is outlined in Algorithm 1 and operates as follows. A spiral is initiated at the start location. The horizontal spacing of the spiral is manually selected to be the expected size of the feature in question. This insures features of the expected size are seen during this initial survey. During this spiral the vehicle completes vertical profiles through the extent of the water column. When the max plume strength value of a single profile exceeds the specified threshold, $plume_t$ in Algorithm 1, the second phase of surveys begins. The height of the detected feature, p_h, is determined by binning the data from the vertical profile, p_d, at a 10 m resolution and selecting the bin with the largest average value. The subsequent surveys are performed at a depth of p_h. This is in contrast to the 3-phase strategy outlined in [German et al. 2008] because of our focus on search in the non-buoyant plume.

During the second phase of surveys, the search space is partitioned into bins, $survey\_bins$, of size $spacing_0$. These bins are separated into four quadrants centered on the corner of the bin closest to the location of the plume detection. A dynamic "lawnmower" survey is executed in each of the four quadrants. The dynamic lawnmower algorithm is outlined in Algorithm 2. The spacing of the lawnmower pattern, $track\_spacing$, is specified beforehand. The direction of the lawnmower pattern is defined by $along\_track$ and $across\_track$. Each track line of the lawnmower pattern consists of sections with length equal to the spacing. At least $min\_sections$ sections are be completed per track line. If $sections\_limit$ sections have average plume strengths below $plume_t$ and the sections have monotonically decreasing average plume strengths, then the track line is completed and the next track line is commenced. $min\_sections$ and $sections\_limit$ are manually specified search parameters. If the maximum value of an entire track line is less than $plume_t$ then the current lawnmower survey is ended and the next begins. The data from each dynamic lawnmower is binned into $survey\_bins$.

An example dynamic lawnmower is shown in Figure 5. The plot is subdivided into track line sections. The average plume strength is listed in each section; a green background indicates that the average plume strength is greater than the specified threshold, $plume_t$. Two boundaries to the survey are shown. Upon reaching the right-most boundary, the vehicle completes the current trackline. The boundaries correspond to the shared edges of the four quadrants defined during the search process.

Upon the completion of each dynamic lawnmower, local maxima of $survey\_bins$ are found. A maximum is declared when the 8 neighboring bins of the same resolution have a max plume detection value less than that of the center bin. Some a maximum has been found a nested "lawnmower" survey begins. An example of this process is shown in Figure 6. The local maximum — shown in green — and its neighbors are subdivided into smaller bins with one-third the side length of their parents. A lawnmower with spacing equal to one-third that of the previous lawnmower survey and with track lines centered on each row of nested bins is initiated. The new nested lawnmower survey covers the local maximum and all surrounding neighbors. If multiple local maxima have been found, they are prioritized on plume strength. This process repeats recursively until a survey spacing of $final\_spacing$, is reached. If no local

maxima are found during a dynamic lawnmower, or all local maxima have been exhausted before the survey spacing of $final\_spacing$ is reached, then the dynamic lawnmowers resume. After all dynamic lawnmower surveys are completed the spiral is resumed. Another set of dynamic lawnmowers is started if a plume is detected outside of the previously searched area.

Algorithm 1 Autonomous Nested Search

procedure NESTED_SEARCH
  $plans \leftarrow$ empty stack
  $visited \leftarrow$ empty set
  $plans.push(spiral)$
  $survey\_bins \leftarrow$ bins of size $spacing_0$
  while $plans.size > 0$ and not timed out **do**
    Execute or Continue $plans.top()$
    if executing spiral **then**
      Wait until end of vertical profile
      $p_d \leftarrow$ Get data from profile
      $d \leftarrow max(p_d)$
      if $d >= plume_t$ and $d.location$ not explored **then**
        $bins \leftarrow profile\_data$ binned at 10 meters and averaged
        $p_h \leftarrow max(bins).height$
        $(x, y) \leftarrow$ bin corner closest to $d.position$
        $plans.push(dynamic\_lawnmower(x, y, p_h, 90°, 0°, spacing_0))$
        $plans.push(dynamic\_lawnmower(x, y, p_h, -90°, 0°, spacing_0))$
        $plans.push(dynamic\_lawnmower(x, y, p_h, -90°, 180°, spacing_0))$
        $plans.push(dynamic\_lawnmower(x, y, p_h, 90°, 180°, spacing_0))$
        Execute $plans.top()$
    else
      while $plans.top()$ is not completed **do**
        Wait
      $survey\_data \leftarrow$ Get data from latest survey
      $survey\_bins.add\_data(survey\_data)$
      $maxima \leftarrow get\_bin\_maxima(survey\_bins)$
      sort $maxima$
      for bin in $maxima$ **do**
        if bin not in $visited$ **then**
          Partition bin and $bin.neighbors()$
          $visited.add(bin)$
          $plans.push(nested\_lawnmower(bin))$
          break
    while $plans.size > 0$ and $plans.top()$ is complete **do**
      $f \leftarrow plans.pop()$
      if $f.spacing < final\_spacing$ and f contains vent source **then**
        return Success
  return Failure

Algorithm 2 Execute Dynamic Lawnmower

procedure EXECUTE_DYNAMIC_LAWNMOWER(x, y, h , along_track, across_track, track_spacing)
  $start\_x \leftarrow x + cos(along\_track) * track\_spacing/2$
  $start\_y \leftarrow y + sin(across\_track) * track\_spacing/2$
  Go to $(start\_x, start\_y, h)$
  $curr\_track \leftarrow 0$
  $curr\_section \leftarrow 0$
  $completed \leftarrow False$
  $section\_data \leftarrow$ empty list
  Start current track line on heading $along\_track$
  while not $completed$ **do**
    Do next section on current track
    $section\_data[curr\_section] \leftarrow$ Get data from last section
    $curr\_section \leftarrow curr\_section + 1$
    if $curr\_section >= min\_sections$ or survey boundary reached **then**
      if $avg(section\_data[i]) < plume_t$ for last $sections\_limit$ sections and monotonically decreasing **then**
        $curr\_track \leftarrow curr\_track + 1$
        if $max(section\_data) < plume\_thresh$ **then**
          $completed \leftarrow True$
          $section\_data \leftarrow$ empty list
          Travel $track\_spacing$ on heading $across\_track$
          if $curr\_track$ is even **then**
            Start next track line on heading $along\_track$
          else
            Start next track line on heading $-along\_track$

Experiment

121 scenarios were completed with the vehicle starting location uniformly varied between $x = [-30000, 30000]$ and $y = [-30000, 30000]$ at intervals of 6000m. Due to the nature of the algorithm and the location of the vent at $(0, 0)$ it is likely that the vehicle will pass directly over the vent source if the start location x and y are multiples of 1000. To mitigate this, a uniformly random value between $[-1500, 1500]$ was added to the x and y values of the starting location. The simulated vehicle has a horizontal and vertical velocity of 1 m/s. The vehicle samples the model at 0.2 hz. The plume detection threshold was set to 0.5. The initial spiral spacing was set to 5000 m and the initial dynamic lawnmower spacing was set to 4000 m. The dynamic lawnmower parameters $min\_sections$ and $sections\_limit$ are set to 4 and 2, respectively. The search parameters were selected based on preliminary results. More work investigating search parameters is necessary.

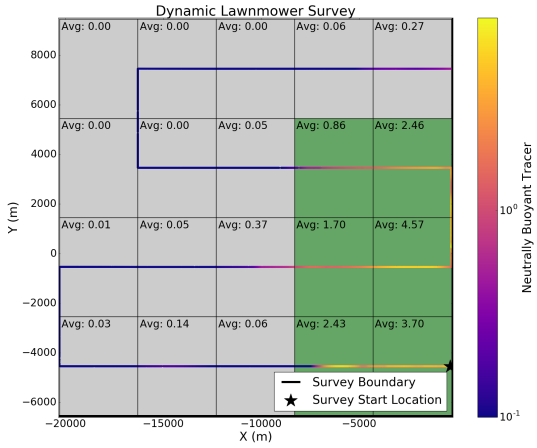

Figure 5: Plot showing an example dynamic lawnmower survey. The survey area is partitioned into regions representing sections of each track line. Regions shaded green have an average plume strength over the specified threshold. The average value is labeled in the upper left corner of each region. The two survey boundaries are shown as thick black lines on the right and bottom of the plot. The starting location is marked with a black star.

Results

87% of the simulation scenarios successfully found the vent location within 28 days. Figure 7 shows the time each run took to successfully find the vent in black. The runs that failed to find the vent are shown in red. Plot (a) shows the total time while plots (b), (c), and (d) show the time spent on the spiral survey, dynamic lawnmower surveys, and nested lawnmower surveys respectively. Figures 8, 9, and 10 show an example run plotting a top down view and a 3d view of the passive tracer (dye) value from the model, and a top down view of the survey types during the run, respectively.

We see a slight correlation between the distance and total time on successful runs. When this is decomposed into the different stages of the algorithm we see this correlation stronger within the spiral surveys while not at all in the lawn-

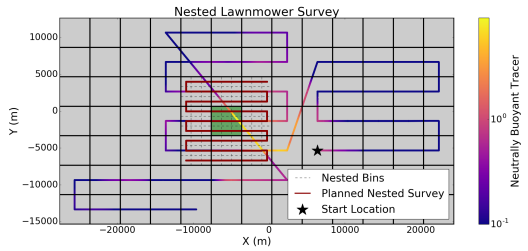

Figure 6: Plot showing an example of the planning process for a single nested lawnmower in one of the four quadrants. The search space is divided into square bins with sides equal to the lawnmower spacing. Upon finding a local maximum bin, the bin and all its neighbors are subdivided into nested bins of one-third the side length. A lawnmower pattern is then executed such that each track line is centered on a row of bins. The vehicle path and observed tracer is plotted. The planned nested lawnmower is show in dark red. The starting location is marked with a black star.
. Note that the measured passive tracer does not remain the same on subsequent measurements of the same location due to the temporal variation in fluid concentrations.

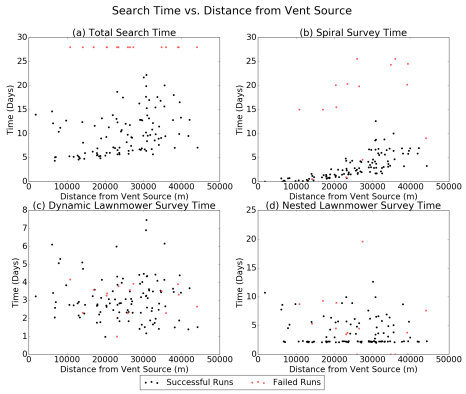

Figure 7: Plots showing the time to find the vent source compared to the distance from the vent source. The runs that successfully find the vent within 28 days are show in black. The failed runs are shown in red. Panel (a) plots the total time spent during the search. Panel (b), (c), and (d) decompose the time into the spiral survey, dynamic lawnmower surveys, and nested surveys respectively

mower surveys. No correlation is seen between the failed surveys and the distance from the vent, indicating that the cause of the failure is not related to distance. This method does not have a set distance in which it is feasible, starting further from the vent location would only require longer search times. Search times can be minimized by selecting appropriate values for the survey spacing parameters.

Upon initial investigation into the failed scenarios we see that the spiral surveys always detect the plume and initiate lawnmower surveys. Two failure modes are then observed in the lawnmower surveys. First, plume strength contours are not closed by the dynamic lawnmower survey. As such, they are not investigated by the nested lawnmower survey. Second, local maxima are not seen at the vent location. This could be caused by the temporal variation of the plume or from using constant depth, as apposed to constant density, lawnmower surveys.

Future Work

The planning method has many areas which could use further investigation. The lawnmower surveys could be improved by guaranteeing that contours will be closed, resulting in less failed searches. The non-buoyant plume is positioned at a constant density, not depth. As such, a fixed depth search is not ideal. In addition, the plume height can vary temporally on the order of 100 m over a tidal cycle on Earth [Rudnicki and German 2002]. A long duration search strategy, with respect to the tidal cycle, should be able to address this temporal variation. Improved search in the vertical direction would insure that the vehicle maintains contact with the strongest part of the plume. Temporal variations in the lateral direction should also be accounted for. This may be particularly important for slower vehicles, perhaps less so if they only move relative to the water, rather than relative to the ground or icy shell. Other geometric search patterns and other search strategies such as gradient search or biologically inspired approaches can be implemented and tested. Automated tuning of search parameters could improve results. Vehicle resource considerations can be incorporated into the planner. More intelligent path planning can be implemented to reduce resource consumption while performing multiple surveys. Hydrothermal activity is one potential target for a submersible; investigation into other targets and the development of a search approach capable of prioritizing multiple target types would be beneficial.

Currently, the vehicle simulation is rudimentary. Realistic models for sensors such as temperature, optical backscatter, and chemical sensors can be developed. Vehicle resources such as power and data capacity can be implemented. Finally, the vehicles motion model can be improved by advecting the vehicle according to the currents in the model.

The data volume collected by the vehicle far exceeds the communication throughput capabilities. Therefore, a method of summarizing the data collected needs to be developed. A number of spacecraft have implemented systems for this purpose. The Autonomous Sciencecraft Experiment used onboard science algorithms to summarize, delete, and prioritize data for downlink [Chien et al. 2005]. The onboard product generation for the Earth Observing-1 mission serves as a predecessor to the proposed HyspIRI Intelligent Payload Module [Chien et al. 2013]. The Mars Exploration Rover's (MER) WATCH system processes imagery to detect dust devils and send summarized data products to Earth [Castano et al. 2008]. The AEGIS system processes onboard imagery to autonomously retarget science instruments on the Mars Science Laboratory [Estlin et al. 2014] and MER [Estlin et al. 2012].

More simulation runs varying search parameters such as starting location, plume detection threshold, and survey

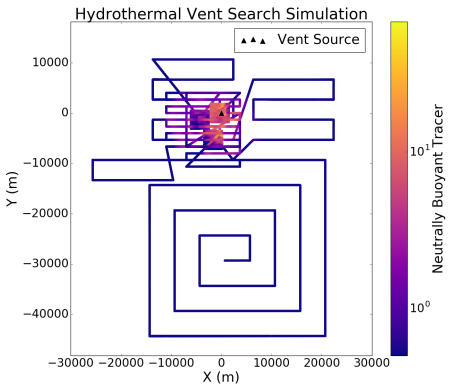

Figure 8: Top down plot showing the passive tracer (dye) as seen by the vehicle from a scenario starting at x=710, y=-29337. The vent source location is shown as a black triangle at (0,0).

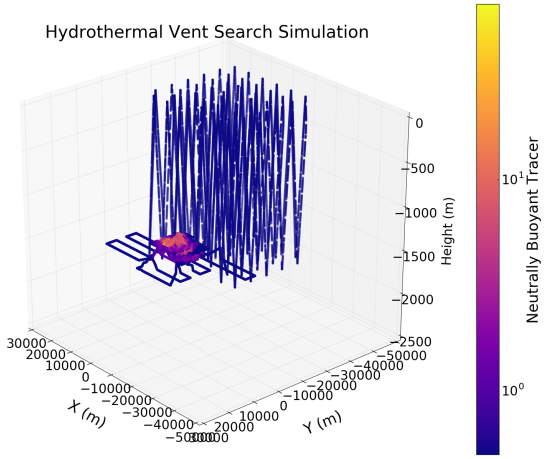

Figure 9: 3d view plot showing the passive tracer (dye) as seen by the vehicle from a scenario starting at x=710, y=-29337.

spacing would allow for a better understanding of the presented search strategy. Another plume dispersal model, either of a different region or with different plume parameters could be developed. Real world tests in well studied areas such as Axial Seamount would further validate the approach.

Conclusion

We developed an autonomous nested search based on the current manual three-phase search method [German et al. 2008], as well as a realistic simulation environment in which to test search strategies for the localization of hydrothermal venting. This simulation environment allows for testing at much larger spatial scales than has been investigated for other autonomous approaches. Search parameters, such as survey resolution and search location, allow for manual fine tuning of the search process based on the observed data, allowing for a human-in-the-loop model when possible. We

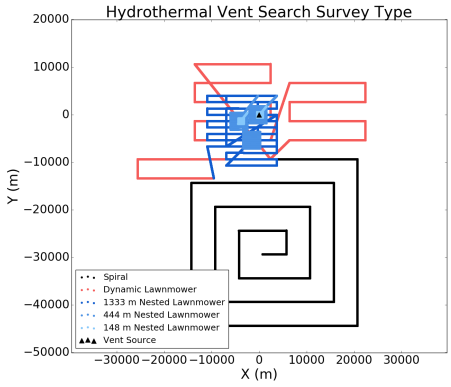

Figure 10: Plots showing the types of surveys performed on a scenario starting at x=710, y=-29337. The spiral survey is shown is black, the dynamic lawnmower surveys are red, and the nested lawnmower surveys are differing shades of blue with darker shades as surveys with larger spacing. The vent source location is shown as a black triangle at (0,0).

performed 121 scenarios with varying start locations, of which 87% were able to successfully find the hydrothermal vent within 28 days.

Acknowledgments

Portions of this work were performed at the Jet Propulsion Laboratory, California Institute of Technology, under contract with the National Aeronautics and Space Administration.

References

Baker, E. T., and German, C. R. 2004. On the global distribution of hydrothermal vent fields. *Mid-ocean ridges* 245–266.

Baker, E. T.; German, C. R.; and Elderfield, H. 1995. Hydrothermal plumes over spreading-center axes: Global distributions and geological inferences. *Seafloor hydrothermal systems: Physical, chemical, biological, and geological interactions* 47–71.

Branch, A.; Flexas, M. M.; Claus, B.; Clark, E. B.; Thompson, A. F.; Chien, S.; Kinsey, J. C.; Fratantoni, D. M.; Zhang, Y.; Kieft, B.; Hobson, B.; and Chavez, F. P. 2018. Front delineation and tracking with multiple underwater vehicles. *J. Field Robotics* submitted.

Castano, A.; Fukunaga, A.; Biesiadecki, J.; Neakrase, L.; Whelley, P.; Greeley, R.; Lemmon, M.; Castano, R.; and Chien, S. 2008. Automatic detection of dust devils and clouds on mars. *Machine Vision and Applications* 19(5-6):467–482.

Chen, C.; Liu, H.; and Beardsley, R. C. 2003. An unstructured grid, finite-volume, three-dimensional, primitive equations ocean model: Application to coastal ocean and estuaries. *Journal of Atmospheric and Oceanic Technology* 20(1):159–186.

Chien, S.; Sherwood, R.; Tran, D.; Cichy, B.; Rabideau, G.; Castano, R.; Davis, A.; Mandl, D.; Trout, B.; Shulman, S.; et al. 2005. Using autonomy flight software to improve science return on earth observing one. *Journal of Aerospace Computing, Information, and Communication* 2(4):196–216.

Chien, S.; Mclaren, D.; Tran, D.; Davies, A. G.; Doubleday, J.; and Mandl, D. 2013. Onboard product generation on earth observing one: a pathfinder for the proposed hyspiri mission intelligent payload module. *IEEE Journal of Selected Topics in Applied Earth Observations and Remote Sensing* 6(2):257–264.

Cruz, N. A., and Matos, A. C. 2010. Adaptive sampling of thermoclines with autonomous underwater vehicles. In *OCEANS 2010*, 1–6. IEEE.

Cruz, N. A., and Matos, A. C. 2014. Autonomous tracking of a horizontal boundary. In *Oceans-St. John's, 2014*, 1–6. IEEE.

Curtin, T. B., and Bellingham, J. G. 2009. Progress toward autonomous ocean sampling networks. *Deep Sea Research Part II: Topical Studies in Oceanography* 56(3):62 – 67. AOSN II: The Science and Technology of an Autonomous Ocean Sampling Network.

Curtin, T. B.; Bellingham, J. G.; Catipovic, J.; and Webb, D. 1993. Autonomous oceanographic sampling networks. *Oceanography* 6(3):86–94.

Das, J.; Py, F.; Maughan, T.; OReilly, T.; Messié, M.; Ryan, J.; Sukhatme, G. S.; and Rajan, K. 2012. Coordinated sampling of dynamic oceanographic features with underwater vehicles and drifters. *The International Journal of Robotics Research* 31(5):626–646.

Eriksen, C. C.; Osse, T. J.; Light, R. D.; Wen, T.; Lehman, T. W.; Sabin, P. L.; Ballard, J. W.; and Chiodi, A. M. 2001. Seaglider: A long-range autonomous underwater vehicle for oceanographic research. *IEEE J. Oceanic Eng.* 26:424436.

Estlin, T. A.; Bornstein, B. J.; Gaines, D. M.; Anderson, R. C.; Thompson, D. R.; Burl, M.; Castano, R.; and Judd, M. 2012. Aegis automated science targeting for the mer opportunity rover. *ACM Transactions on Intelligent Systems and Technology (TIST)* 3(3):50.

Estlin, T.; Gaines, D.; Bornstein, B.; Schaffer, S.; Tompkins, V.; Thompson, D. R.; Altinok, A.; Anderson, R. C.; Burl, M.; Castaño, R.; et al. 2014. Automated targeting for the msl rover chemcam spectrometer. In *12th International Symposium on Artificial Intelligence, Robotics, and Automation in Space (i-SAIRAS)*, 17–19.

Farrell, J. A.; Pang, S.; and Li, W. 2005. Chemical plume tracing via an autonomous underwater vehicle. *IEEE Journal of Oceanic Engineering* 30(2):428–442.

Ferri, G.; Jakuba, M. V.; and Yoerger, D. R. 2010. A novel trigger-based method for hydrothermal vents prospecting using an autonomous underwater robot. *Autonomous Robots* 29(1):67–83.

Flexas, M. M.; Troesch, M. I.; Chien, S.; Thompson, A. F.; Chu, S.; Branch, A.; Farrara, J. D.; and Chao, Y. 2018. Autonomous sampling of ocean submesoscale fronts with ocean gliders and numerical model forecasting. *Journal of Atmospheric and Oceanic Technology* 35(3):503–521.

German, C., and Seyfried, W. 2014. Hydrothermal processes. *Treatise on geochemistry* 8:191–233.

German, C. R.; Yoerger, D. R.; Jakuba, M.; Shank, T. M.; Langmuir, C. H.; and Nakamura, K.-i. 2008. Hydrothermal exploration with the autonomous benthic explorer. *Deep Sea Research Part I: Oceanographic Research Papers* 55(2):203–219.

Godin, M. A.; Zhang, Y.; Ryan, J. P.; Hoover, T. T.; and Bellingham, J. G. 2011. Phytoplankton bloom patch center localization by the tethys autonomous underwater vehicle. In *OCEANS'11 MTS/IEEE KONA*, 1–6.

Haley, P.; Lermusiaux, P.; Robinson, A.; Leslie, W.; Logoutov, O.; Cossarini, G.; Liang, X.; Moreno, P.; Ramp, S.; Doyle, J.; Bellingham, J.; Chavez, F.; and Johnston, S. 2009. Forecasting and reanalysis in the monterey bay/california current region for the autonomous ocean sampling network-ii experiment. *Deep Sea Research Part II: Topical Studies in Oceanography* 56(3):127 – 148. AOSN II: The Science and Technology of an Autonomous Ocean Sampling Network.

Hsu, H.-W.; Postberg, F.; Sekine, Y.; Shibuya, T.; Kempf, S.; Horányi, M.; Juhász, A.; Altobelli, N.; Suzuki, K.; Masaki, Y.; et al. 2015. Ongoing hydrothermal activities within enceladus. *Nature* 519(7542):207.

Jakuba, M., and Yoerger, D. R. 2008. Autonomous search for hydrothermal vent fields with occupancy grid maps. In *Proc. of ACRA*, volume 8, 2008.

Leonard, N. E.; Paley, D. A.; Lekien, F.; Sepulchre, R.; Fratantoni, D. M.; and Davis, R. E. 2007. Collective motion, sensor networks, and ocean sampling. *Proceedings of the IEEE* 95(1):48–74.

Leonard, N. E.; Paley, D. A.; Davis, R. E.; Fratantoni, D. M.; Lekien, F.; and Zhang, F. 2010. Coordinated control of an underwater glider fleet in an adaptive ocean sampling field experiment in monterey bay. *Journal of Field Robotics* 27(6):718–740.

Magazzeni, D.; Py, F.; Fox, M.; Long, D.; and Rajan, K. 2014. Policy learning for autonomous feature tracking. *Autonomous Robots* 37(1):47–69.

Nakamura, K.; Veirs, S.; Sarason, C. P.; McDuff, R. E.; Stahr, F.; Yoerger, D. R.; and Bradley, A. M. 2000. Electrochemical signals in rising buoyant plumes and tidally oscillating plumes at the main endeavour vent field, juan de fuca ridge. *EOS, Transactions of the American Geophysical Union* 81(48).

National Aeronautics and Space Administration. 2018. Ocean worlds.

Pang, S. 2010. Plume source localization for auv based autonomous hydrothermal vent discovery. In *OCEANS 2010*, 1–8. IEEE.

Petillo, S.; Schmidt, H.; and Balasuriya, A. 2012. Constructing a distributed auv network for underwater plume-tracking operations. *International Journal of Distributed Sensor Networks* 2012:Article ID 191235, 12pp.

Ramp, S.; Davis, R.; Leonard, N.; Shulman, I.; Chao, Y.; Robinson, A.; Marsden, J.; Lermusiaux, P.; Fratantoni, D.; Paduan, J.; Chavez, F.; Bahr, F.; Liang, S.; Leslie, W.; and Li, Z. 2009. Preparing to predict: The second autonomous ocean sampling network (aosn-ii) experiment in the monterey bay. *Deep Sea Research Part II: Topical Studies in Oceanography* 56(3):68 – 86. AOSN II: The Science and Technology of an Autonomous Ocean Sampling Network.

Rudnicki, M. D., and German, C. R. 2002. Temporal variability of the hydrothermal plume above the kairei vent field, 25 s, central indian ridge. *Geochemistry, Geophysics, Geosystems* 3(2).

Saigol, Z.; Dearden, R.; Wyatt, J.; and Murton, B. 2010. Belief change maximisation for hydrothermal vent hunting using occupancy grids. In *Proceedings of the Eleventh Conference Towards Autonomous Robotic Systems (TAROS-10)*, 247–254.

Speer, K. G., and Rona, P. A. 1989. A model of an atlantic and pacific hydrothermal plume. *Journal of Geophysical Research: Oceans* 94(C5):6213–6220.

Sun, L.; Li, Y.; Yan, S.; Wang, J.; and Chen, Z. 2016. Thermocline tracking using a portable autonomous underwater vehicle based on adaptive threshold. In *OCEANS 2016-Shanghai*, 1–4. IEEE.

Tian, Y.; Zhang, A.; Li, W.; Yu, J.; Li, Y.; and Zeng, J. 2014. A behavior-based planning strategy for deep-sea hydrothermal plume tracing with autonomous underwater vehicles. In *OCEANS 2014-TAIPEI*, 1–10. IEEE.

Troesch, M.; Chien, S. A.; Chao, Y.; and Farrara, J. D. 2016. Planning and control of marine floats in the presence of dynamic, uncertain currents. In *International Conference on Automated Planning and Scheduling*, 431–440.

Turner, J. S. 1979. *Buoyancy effects in fluids*. Cambridge University Press.

Veirs, S. R. 2003. *Heat flux and hydrography at a submarine volcano: Observations and models of the Main Endeavour vent field in the northeast Pacific*. Ph.D. Dissertation, University of Washington.

Waite, J. H.; Glein, C. R.; Perryman, R. S.; Teolis, B. D.; Magee, B. A.; Miller, G.; Grimes, J.; Perry, M. E.; Miller, K. E.; Bouquet, A.; Lunine, J. I.; Brockwell, T.; and Bolton, S. J. 2017. Cassini finds molecular hydrogen in the enceladus plume: Evidence for hydrothermal processes. *Science* 356(6334):155–159.

Yoerger, D. R.; Bradley, A. M.; Jakuba, M. V.; Tivey, M. A.; German, C. R.; Shank, T. M.; and Embley, R. W. 2007a. Mid-ocean ridge exploration with an autonomous underwater vehicle.

Yoerger, D. R.; Jakuba, M.; Bradley, A. M.; and Bingham, B. 2007b. Techniques for deep sea near bottom survey using an autonomous underwater vehicle. *The International Journal of Robotics Research* 26(1):41–54.

Zhang, Y.; Bellingham, J. G.; Godin, M.; Ryan, J. P.; McEwen, R. S.; Kieft, B.; Hobson, B.; and Hoover, T. 2010. Thermocline tracking based on peak-gradient detection by an autonomous underwater vehicle. In *OCEANS 2010*, 1–4. IEEE.

Zhang, Y.; Bellingham, J. G.; Ryan, J. P.; Kieft, B.; and Stanway, M. J. 2013. Two-dimensional mapping and tracking of a coastal upwelling front by an autonomous underwater vehicle. *Proc. MTS/IEEE Oceans'13* 1–4.

Zhang, Y.; Bellingham, J. G.; Ryan, J. P.; Kieft, B.; and Stanway, M. J. 2016. Autonomous four-dimensional mapping and tracking of a coastal upwelling front by an autonomous underwater vehicle. *Journal of Field Robotics* 33(1):67–81.

Zheng, L., and Weisberg, R. H. 2012. Modeling the west florida coastal ocean by downscaling from the deep ocean, across the continental shelf and into the estuaries. *Ocean Modelling* 48:10 – 29.